ISSN 1990-7931, Russian Journal of Physical Chemistry B, 2025, Vol. 19, No. 5, pp. 1222–1238. © Pleiades Publishing, Ltd., 2025.

CHEMICAL PHYSICS OF NANOMATERIALS

Efficiency Probing of GaInP/GaInAs-Based Solar Cells through Synergy of Silicon, Zinc or Silver Elements: A First-Priciples Study

F. Mollaamin*

Department of Biomedical Engineering, Faculty of Engineering and Architecture, Kastamonu University, Kastamonu, Turkey
**e-mail: fmollaamin@kastamonu.edu.tr*

Received April 6, 2025; revised May 16, 2025; accepted May 20, 2025

Abstract—Heteroclusters of (Si,Zn,Ag)-Doped GaInP/GaInAs can attract considerable attention for storage energy in solar cells. A comprehensive investigation on energy grabbing by GaInP, Si@GaInP, Zn@GaInP, Ag@GaInP, GaInAs, Si@GaInAs, Zn@GaInAs, Ag@GaInAs was carried out including using DFT computations at the CAM–B3LYP–D3/6-311+G(*d*, *p*) level of theory. Electromagnetic and thermodynamic properties of GaInP, Si@GaInP, Zn@GaInP, Ag@GaInP, GaInAs, Si@GaInAs, Zn@GaInAs, Ag@GaInAs heteroclusters have been evaluated. The hypothesis of the energy adsorption phenomenon was confirmed by density distributions of CDD, TDOS and ELF for GaInP, Si@GaInP, Zn@GaInP, Ag@GaInP, GaInAs, Si@GaInAs, Zn@GaInAs, Ag@GaInAs heteroclusters. In GaInP and GaInAs, the photo excited electrons and holes are strongly bounded by the excitons because of their large exciton binding energy as $E^{o}_{Ag@GaInX} > E^{o}_{Zn@GaInX} > E^{o}_{Si@GaInX}$ (X = P or As) due to its efficient exciton dissociation. Therefore, it can be considered that zinc and silver atoms in the functionalized Zn@GaInP/As and Ag@GaInP/As might have more impressive sensitivity for accepting the electrons in the process of energy adsorption mechanism. The changes of Gibbs free energy versus dipole moment could detect the maximum efficiency of Ag@GaInP and Ag@GaInAs heteroclusters for energy storage in the solar cells through $\Delta G^{o}_{f,Ag@GaInP} = -134.9792 \times 10^3$ kcal/mol and $\Delta G^{o}_{f,Ag@GaInAs} = -132.1931 \times 10^3$ kcal/mol, respectively. As a matter of fact, it can be observed that doped heteroclusters of Ag@GaInX and Zn@GaInX (X = P or As) might ameliorate the capability of GaInX (X = P or As) in solar cells for energy storage.

Keywords: heterocluster, solar cells, energy saving, materials modeling

DOI: 10.1134/S1990793125700915

1. INTRODUCTION

The semiconductor of Gallium nitride (GaN) is a very hard material with wide bandgap applied in a variety of technologies, including optoelectronic, high-power electronics and light-emitting diodes, partly due to its favorable thermal properties [1–4]. The nitrides of group III in periodic table have low sensitivity to ionizing radiation which make them appropriate materials for solar cell arrays for satellites. Therefore, space applications could also benefit as devices have shown stability in high radiation environments. Because GaN transistors can operate at much higher temperatures and work at much higher voltages than gallium arsenide (GaAs) transistors, they make ideal power amplifiers at microwave frequencies. In addition, GaN offers promising characteristics for THz devices. Due to high power density and voltage breakdown limits GaN is also emerging as a promising candidate for 5G cellular base station applications [5–8].

GaN with a high crystalline quality can be obtained by depositing a buffer layer at low temperatures [9, 10]. Such high-quality GaN led to the discovery of *p*-type GaN [11], *p–n* junction blue/UV-LEDs [5] and room-temperature stimulated emission [12]. This has led to the commercialization of high-performance blue LEDs and long-lifetime violet laser diodes, and to the development of nitride-based devices such as UV detectors and high-speed field-effect transistors [13]. GaN-based metal–oxide–semiconductor field-effect transistor (MOSFET) and metal–semiconductor field-effect transistor (MESFET) transistors also offer advantages including lower loss in high power electronics, especially in automotive and electric car applications [14]. The U.S. Army Research Laboratory (ARL) provided the first measurement of the high field electron velocity in GaN in 1999 [15]. Scientists at ARL experimentally obtained a peak steady-state velocity of 1.9×10^7 cm/s, with a transit time of 2.5 ps, attained at an electric field of 225 kV/cm. With this information, the electron mobility was calculated, thus providing data for the design of GaN devices.

Recently, a review article was focused on the interaction between nanoparticles of the sensitive layer, and its effect on the structure, sensitivity, and selectivity of semiconductor sensor systems. Different mechanisms of interaction between nanoparticles in metal oxide composites have been considered, containing the incorporation of metal ions of one component into the structure of another, heterocontacts between various nanoparticles, and core–shell systems, as well as their influence on the characteristics of gas sensors [16].

Solar cells of ternary alloys such as indium gallium nitride (InGaN) are attracting interest due to the tunable direct band gap energy of InGaN covering the whole solar spectrum ranging from 0.7 eV (band gap energy of InN) to 3.4 eV (band gap energy of GaN) [17, 18], as well as superior photovoltaic characteristics of InGaN including high absorption coefficients ($\sim 105\ cm^{-1}$) [19] and high carrier mobility. Moreover, high stability (thermal and chemical) and superior radiation resistance of InGaN alloys allow operation of InGaN-based devices in extreme conditions such as space and terrestrial applications [17, 20]. InGaN-based solar cells have been successfully fabricated with low indium contents of the InGaN alloy [21–23]. Lower indium content in InGaN leads to an increase in the band gap energy of InGaN, which in turn results in the absorption of only shorter wavelengths of solar radiation. Hence, to realize high-efficiency InGaN solar cells, the indium content in the InGaN active layer of these solar cells must be increased in order to cover a major part of the solar spectrum. Some researchers have recently proposed the use of dual nanogratings in silicon (crystalline, microcrystalline, and amorphous) and organic solar cells etc. In most of these solar cells, the nanogratings are in direct contact with the active region of the solar cells [24–32].

The ability to perform bandgap engineering with InGaN over a range that provides a good spectral match to sunlight, makes InGaN suitable for solar photovoltaic cells. It is possible to grow multiple layers with different bandgaps, as the material is relatively insensitive to defects introduced by a lattice mismatch between the layers. Metal-doped allows controlled atomic layer-by-layer growth of thin films with almost ideal characteristics enabled by strain relaxation at the first atomic layer. The crystal's lattice structures match up, resembling a perfect crystal, with corresponding luminosity. Ultrafast exciton and charge-carrier dynamics in InGaN/GaN nanowires with and without Rh/Cr_2O_3 nanoparticle decoration have been investigated using femtosecond transient absorption techniques with excitation at 415 nm and white-light probe (450–700 nm) [33]. The researchers reported on the growth and magnetic properties of single crystal Mn-doped GaN, InGaN, and AlGaN films. By optimizing the growth and annealing conditions of Mn-doped III-Nitrides, the researchers have achieved that these ferromagnetic films exhibit hysteresis [34, 35].

Furthermore, an efficient visible-light photoelectrochemical photodetector based on a compact In-rich *n*-InGaN layer activated by *p*-Cu_2O microcrystals operating as photoanode in the self-powered mode was illustrated. The excellent performance was attributed to maximized photocarrier separation in the built-in electric field of the internal *p–n* junction for fully depleted Cu_2O microcrystals with maximized height and the planar geometry, guaranteeing unhindered diffusion of the electrolyte to and from the photoanode surface [36].

Doping obviously reduces indium atoms composition, the aggregation of In–In and induces the deep energy level. This greatly decreases the defects and improves the valence band potential of InGaN nanorods [37]. Composites based on indium oxide containing different amounts of zinc oxide were synthesized by hydrothermal and impregnation methods. The phase composition, structure, and specific surface of the obtained composites are studied by various physicochemical methods. It was indicated that the method of formation has a significant effect on the structural characteristics of the composites, which in turn leads to the implementation of various conduction mechanisms [38–40].

Recently, researchers have proposed an indium-rich InGaN/GaN *p–i–n* thin-film solar cell which incorporates a dual nanograting (NG) structure: Ag nanogratings (Ag-NGs) on the backside of the solar cell and gallium nitride nanogratings (GaN-NGs) on the frontside. Finite-difference time-domain (FDTD) simulation results show that the dual NG structure couples the incident sunlight to the plasmonic and photonic modes, thereby increasing the absorption of the solar cell in a broad spectral range. It is observed that the solar cells having dual nanograting structures have a significant enhancement in light absorption as compared to cells having either no nanogratings or having only the front side nanogratings or only the backside nanogratings [41]. In this paper, it is considered feasible ternary alloys of gallium indium phosphide (GaInP) and Indium gallium arsenide (GaInAs) which are doped with silicon, zinc or silver. This article aims to systematically investigate the key applications of theoretical calculations in energy storage devices, with a particular focus on how these heteroclusters can better elucidate the actual performance of materials and anticipate the challenges and opportunities that may arise in future development.

2. THEORY, MATERIALS AND COMPUTATION

Doping of Si, Zn, or Ag elements on the ternary alloys of GaInP (Fig. 1a) and GaInAs (Fig. 1a') as solar cells were calculated within the framework of first-principles calculation based on density functional theory (DFT) (Figs. 1b, 1b', 1c, 1c', 1d, 1d').

The DFT method presents the electronic density arising from simple superposition of atomic charges ρ_{SAO}, the density obtained by full solution of DFT Kohn–Sham equation ρ_{KS} and the difference of these two:

$$\Delta\rho \equiv \rho_{KS} - \rho_{SAO}. \quad (1)$$

Any superposition of charge of separated atoms has no electric dipole moment, therefore either Kohn–ham density ρ_{KS} or the density difference $\Delta\rho$ may be used for calculation of the polarization and the polarization induced electric field. In principle the results obtained using both approaches should differ only by an error arising from intersection of the subtracted separated atom charge by top and bottom boundaries. The coordinate shift, resulting from the periodic boundary conditions may affect magnitude of the dipole obtained from the integration over simulated volume [42–49].

The rigid potential energy surface using density functional theory [50–55] was performed due to Gaussian 16 revision C.01 program package [56] and GaussView 6.1 [57]. The coordination input for energy storage on the solar cells has applied 6-311+G(*d*, *p*) and EPR–3 basis sets. The NQR method is related to the multipole expansion in Cartesian coordinates as Eq. (2) [58, 59]:

$$V(r) = V(0) + \left[\left(\frac{\partial V}{\partial x_i}\right)_0 x_i\right] + \frac{1}{2}\left[\left(\frac{\partial^2 V}{\partial x_i x_j}\right)_0 x_i x_j\right] + \ldots \quad (2)$$

After that, a simplification on Eq. (6), there are only the second derivatives related to the identical variable for the potential energy [58, 59]:

$$U = -\frac{1}{2}\int_{\mathcal{D}} d^3 r \rho_r \left[\left(\frac{\partial^2 V}{\partial x_i^2}\right)_0 x_i^2\right] = -\frac{1}{2}\int_{\mathcal{D}} d^3 r \rho_r \times \left[\left(\frac{\partial E_i}{\partial x_i}\right)_0 x_i^2\right] = -\frac{1}{2}\left(\frac{\partial E_i}{\partial x_i}\right)_0 \int_{\mathcal{D}} d^3 r\left[\rho(r) x_i^2\right]. \quad (3)$$

There are two parameters which must be gotten from NQR experiments: the quadrupole coupling constant, χ, and asymmetry parameter of the EFG tensor η:

$$\chi = e^2 Q q_{zz}/h, \quad (4)$$

$$\eta = q_{xx} - q_{yy}/q_{zz}, \quad (5)$$

where q_{ii} are ingredients of the EFG tensor at the quadrupole nucleus determined in the EFG principal axes system, Q is the nuclear quadrupole moment, e is the proton charge and h is the Planck's constant [60, 61].

Solid-state NMR spectroscopy is a technique for characterizing atomic level structure in solid materials such as powders, single crystals and amorphous samples and tissues. Solid-state NMR has been successfully used to study metal organic frameworks (MOFS), batteries, and surfaces of nanoporous materials [62–67].

From the DFT calculations, the chemical shielding (CS) tensors have been attained in the principal axes system for estimating the isotropic chemical-shielding (CSI) and anisotropic chemical-shielding (CSA) [68]:

$$\sigma_{iso} = (\sigma_{11} + \sigma_{22} + \sigma_{33})/3, \quad (6)$$

$$\sigma_{aniso} = \sigma_{33} - (\sigma_{22} + \sigma_{11})/2. \quad (7)$$

Figures 1a, 1a', 1b, 1b', 1c, 1c', 1d, 1d' shows the process of energy storage on heteroclusters of GaInP, Si@GaInP, Zn@GaInP, Ag@GaInP, GaInAs, Si@GaInAs, Zn@GaInAs, Ag@GaInAs which is varied to maximize the absorption in the active region. Further, it was optimized the structural parameters of ternary alloys of GaInP or GaInAs which are doped with silicon, zinc or silver towards formation of heteroclusters of Si@GaInP, Zn@GaInP, Ag@GaInP, Si@GaInAs, Zn@GaInAs, Ag@GaInAs for obtaining the highest short-circuit current density in these solar cells [69–71].

3. RESULTS AND DISCUSSION

In this article, the data has evaluated the efficiency of heteroclusters of GaInP, Si@GaInP, Zn@GaInP, Ag@GaInP, GaInAs, Si@GaInAs, Zn@GaInAs, Ag@GaInAs for storage energy in solar cells.

3.1. CDD, TDOS and ELF Analysis

The amounts of charge density differences "CDD" are measured by considering isolated atoms or noninteracting ones. The mentioned approximation can be the lightest to use because the superposition value may be received from the primary status of the self-consistency cycle in the code that carries out the density functional theory (Figs. 2a, 2a', 2b, 2b', 2c, 2c', 2d, 2d') [72]. In Figs. 2a, 2a', the atoms of P/As10, P/As12, P/As14, P/As16, P/As17 from GaInP or GaInAs have shown the fluctuation around –9 to +4.5 Bohr. The atoms of P/As10, P/As14, P/As16, P/As17 from In_8N_9 have indicated the fluctuation around –9 to +5 Bohr for Si@GaInP or Si@GaInAs (Figs. 2b, 2b'). In Figs. 2c, 2c', the atoms of N10, N14 extracted from ternary hereto clusters of Zn@GaInP or Zn@GaInAs have exhibited the fluctuation around –9 to + 5.5 Bohr. Then, the two doped hereto clusters of Ag@GaInP or Ag@GaInAs (Figs. 2d, 2d') with active atoms of P/As10, P/As14, P/As16, P/As7 oscillated around –9 to + 2.5 Bohr.

Squirming the molecular orbital data owing to gaussian graphs of unit altitude and entire width at half maximum (FWHM) of 0.3 eV by GaussSum 3.0.2 [73] have computed total density of states (TDOS). To better understand the different adsorption characteristics

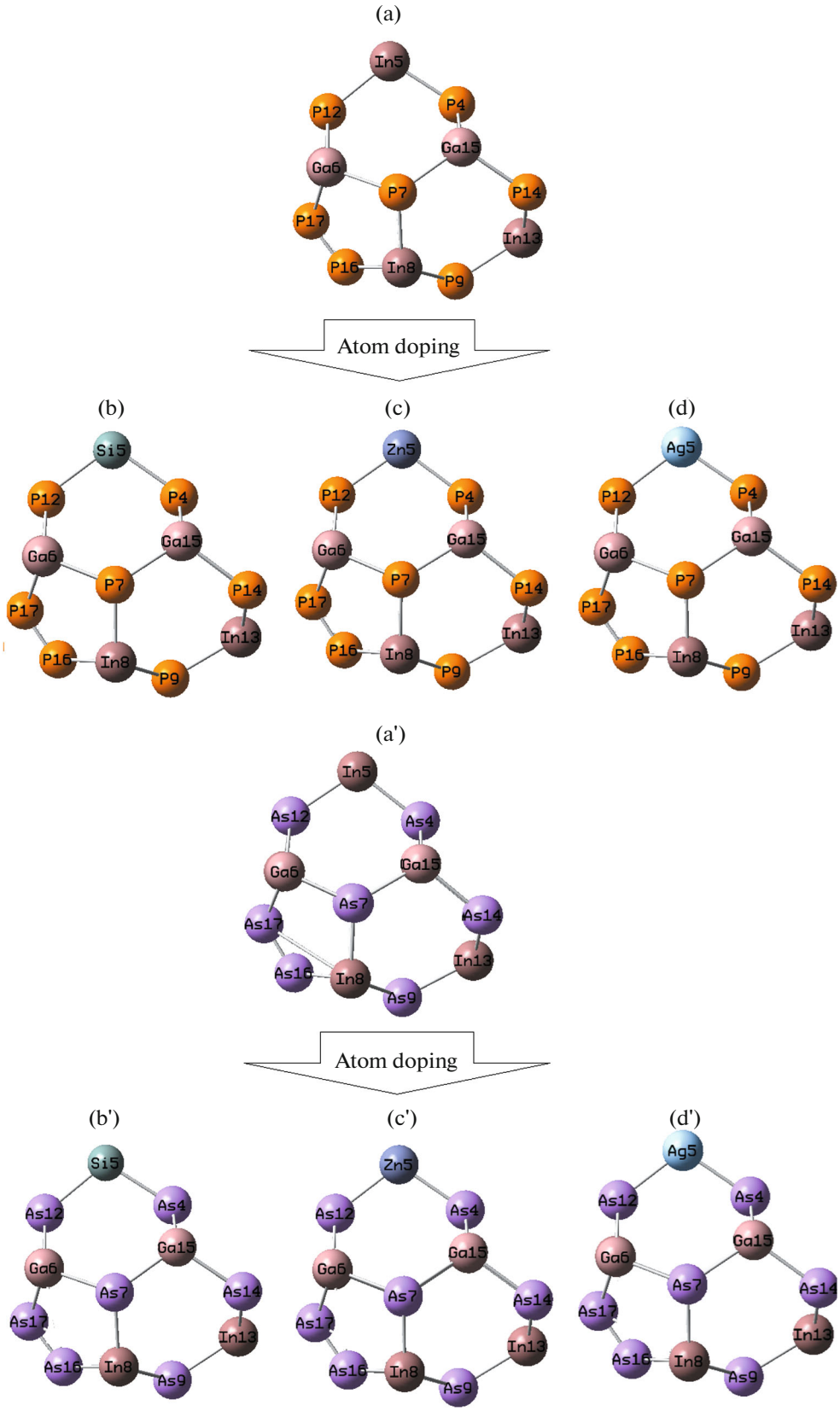

Fig. 1. Application of heteroclusters of (a) GaInP, (b) Si@GaInP, (c) Zn@GaInP, (d) Ag@GaInP, (a') GaInAs, (b') Si@GaInAs, (c') Zn@GaInAs, (d') Ag@GaInAs for energy storage in solar cells using CAM–B3LYP–D3/6-311+G (*d*, *p*) calculation.

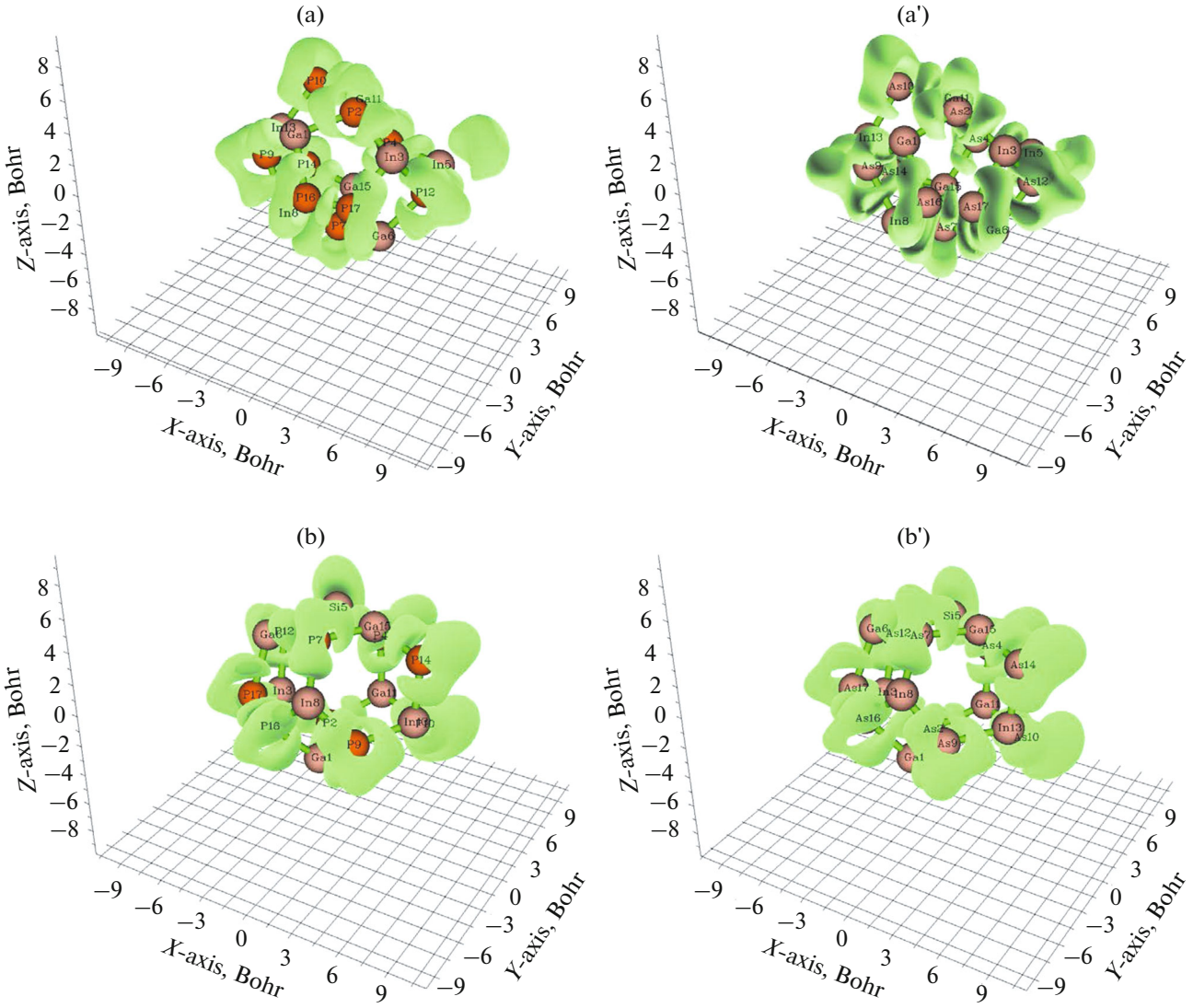

Fig. 2. CDD graphs for heteroclusters of (a) GaInP, (a') GaInAs, (b) Si@GaInP, (b') Si@GaInAs, (c) Zn@GaInP, (c') Zn@GaInAs, (d) Ag@GaInP, (d') Ag@GaInAs.

of GaInP, Si@GaInP, Zn@GaInP, Ag@GaInP, GaInAs, Si@GaInAs, Zn@GaInAs, Ag@GaInAs, total density of states (TDOS) using Multiwfn program [74, 75] has been measured. This parameter can indicate the existence of important chemical interactions often on the convex side (Figs. 3a, 3a', 3b, 3b', 3c, 3c', 3d, 3d'). In an isolated system (such as molecule), the energy levels are discrete, the concept of density of state (DOS) is supposed to be completely valueless in this situation. Therefore, the original total DOS (TDOS) of isolated system can be written as [76]:

$$\mathrm{TDOS}(E) = \sum_i \delta(E - \epsilon_i). \tag{8}$$

$$G(x) = \frac{1}{c\sqrt{2\pi}} e^{\frac{-x^2}{2c^2}} \text{ where } c = \frac{\mathrm{FWHM}}{2\sqrt{2\ln x}}. \tag{9}$$

The maximum energy of TDOS for GaInP (Fig. 3a) and GaInAs (Fig. 3a') with a sharp peak around –0.3 a.u. Figures 3b, 3b' shows the ternary alloys of Si@GaInP and Si@GaInAs with a sharp peak around –0.3 a.u. and a weak peak around –0.4 a.u.

Moreover, the similar amounts of TDOS for Zn@GaInP and Zn@GaInAs with two sharper peak around –0.3 and –0.5 a.u. make these ternary alloys more effective solar cell for adsorption energy (Figs. 3c, 3c'). After doping Ag on GaInP and GaInAs heteroclusters, a sharp peak around –0.7 a.u. has been more clarified (Figs. 3d, 3d'). It is remarkable that the excessive growth technique on doping silicon is a potential approach to designing high efficiency semipolar gallium nitride devices on silicon layers in a long wavelength zone.

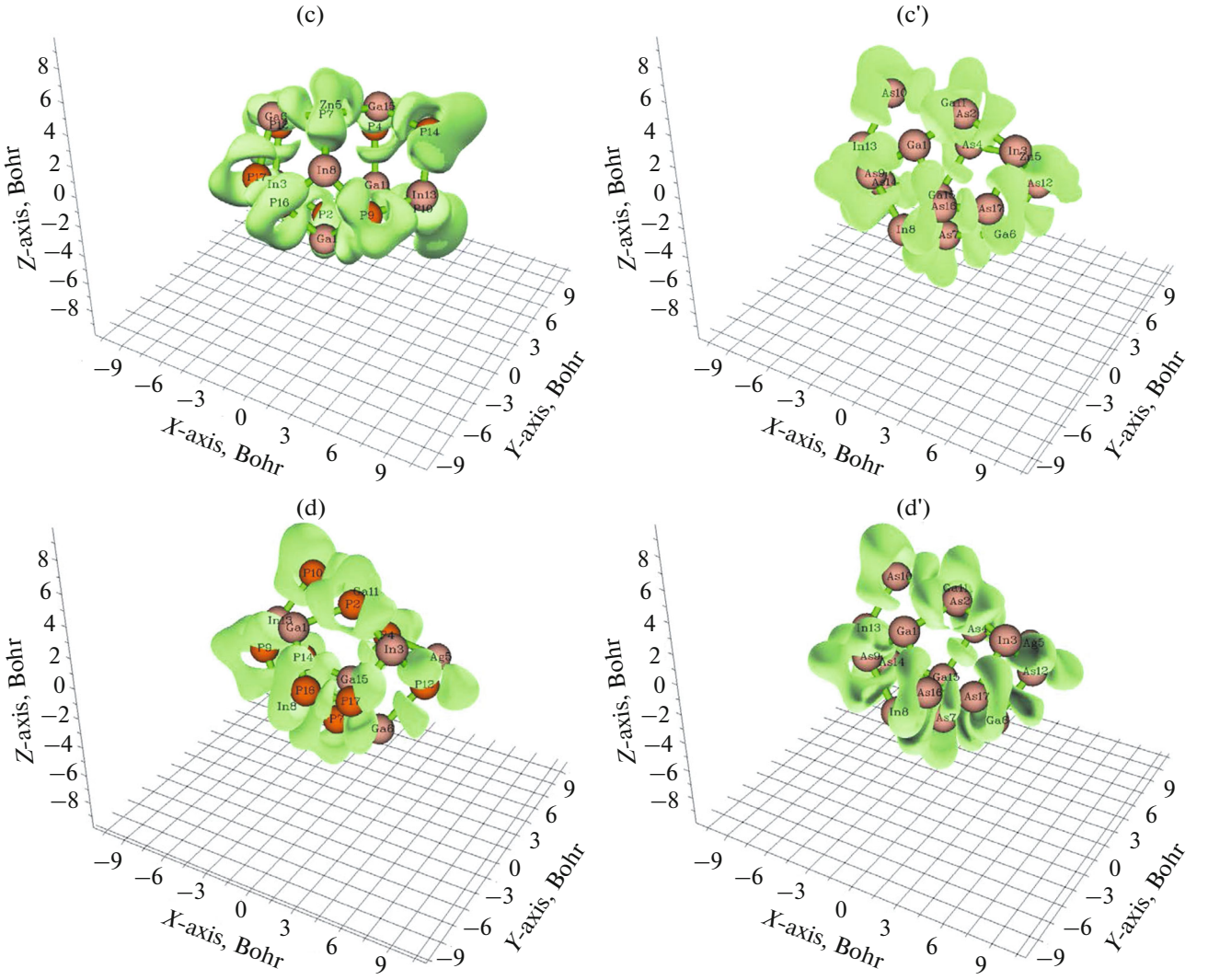

Fig. 2. (Contd.)

Furthermore, a type of scalar fields called electron localization function (ELF) may demonstrate a broad span of bonding samples. Nevertheless, the distinction between deduced/raised electron delocalization/localization into cyclic π-conjugated sets stays encouraging for ELF [77]. The grosser the electron localization is in an area, the more likely the electron movement is restricted within it. Therefore, they might be discerned from the ones away if electrons are totally centralized. As Bader investigated, the zones with large electron localization possess extensive magnitudes of Fermi hole integration. But, with having a six-dimension function for the Fermi hole, it seems hard to be studied directly. Then, Becke and Edgecombe remarked that spherically averaged like spin conditional pair probability possesses a direct correlation with the Fermi hole and proposed the parameter of electron localization function (ELF) in Multiwfn program [75.75] and popularized for spin-polarized procedure [78]:

$$\mathrm{ELF}(r) = \frac{1}{1+[D(r)/D_0(r)]}, \tag{10}$$

where

$$D(r) = \frac{1}{2}\sum_i \eta_i |\nabla\varphi_i(r)|^2 - \frac{1}{8}\left[\frac{|\nabla\rho_\alpha(r)|^2}{\rho_\alpha(r)} + \frac{|\nabla\rho_\beta(r)|^2}{\rho_\beta(r)}\right], \tag{11}$$

and

$$D_0(r) = \frac{3}{10}\left(6\pi^2\right)^{2/3}\left[\rho_\alpha(r)^{5/3} + \rho_\beta(r)^{5/3}\right]. \tag{12}$$

For close-shell system, since $\rho_\alpha = \rho_\beta = (1/2)\rho$, D and $D0$ terms can be simplified as:

$$D(r) = \frac{1}{2}\sum_i \eta_i |\nabla\varphi_i(r)|^2 - \frac{1}{8}\frac{|\nabla\rho(r)|^2}{\rho(r)}, \tag{13}$$

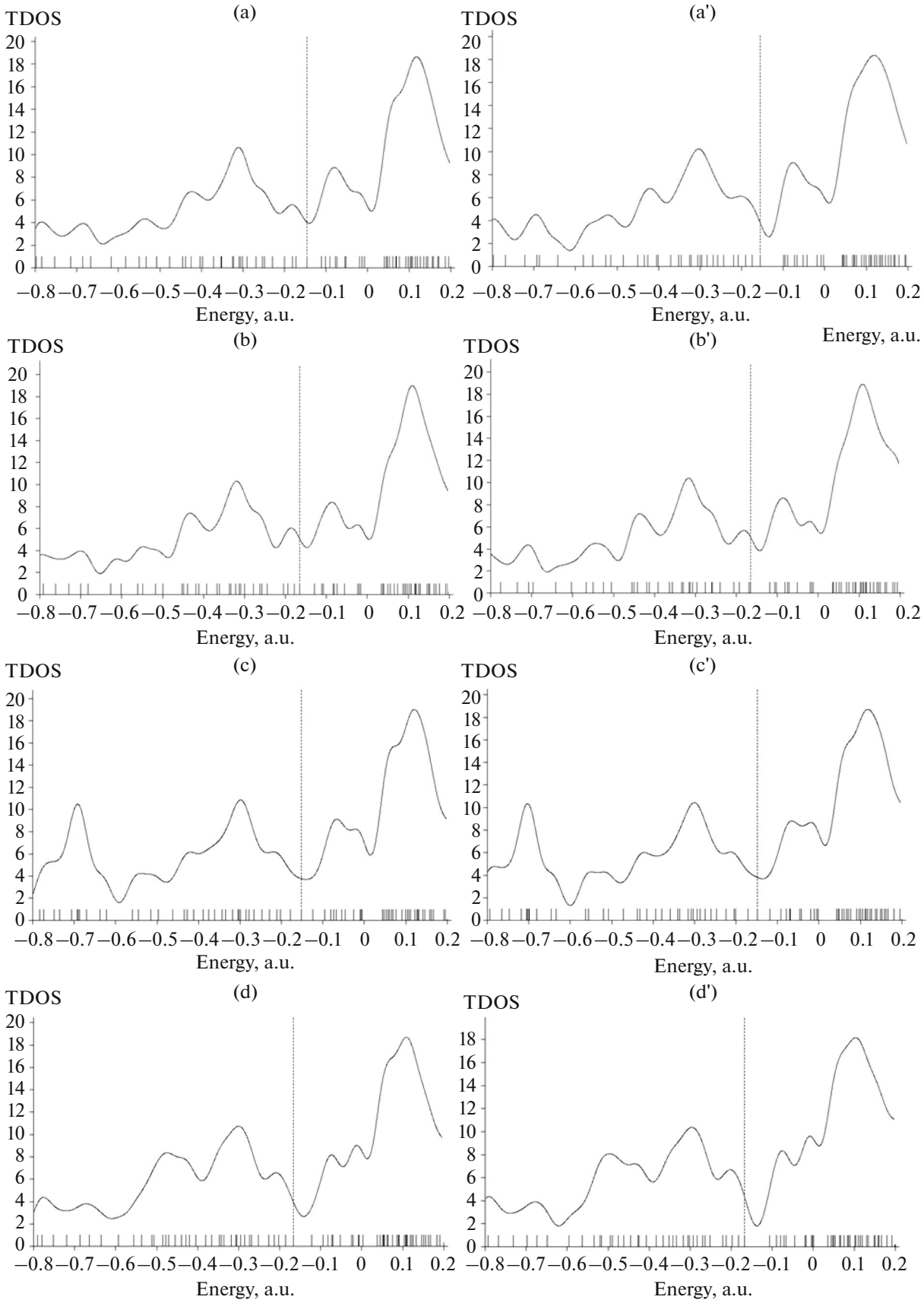

Fig. 3. TDOS graphs of heteroclusters include (a) GaInP, (a') GaInAs, (b) Si@GaInP, (b') Si@GaInAs, (c) Zn@GaInP, (c') Zn@GaInAs, (d) Ag@GaInP, (d') Ag@GaInAs.

and

$$D_0(r) = (3/10)\left(3\pi^2\right)^{2/3} \rho(r)^{5/3}. \quad (14)$$

Regarding kinetic energy, ELF was rechecked to be more punctual for both Kohn–Sham DFT and post-HF wavefunctions [79–85].

In fact, the excess kinetic energy density caused by Pauli repulsion was unfolded by $D(r)$ and $D_0(r)$ may be inspected as Thomas–Fermi kinetic energy density. Because $D_0(r)$ is brough forward the ELF as origin, what the ELF shows is an affiliate localization. The compounds of GaInP, Si@GaInP, Zn@GaInP, Ag@GaInP, GaInAs, Si@GaInAs, Zn@GaInAs, Ag@GaInAs can be defined by ELF graphs owing to exploring their delocalization/localization characterizations of electrons and chemical bonds (Figs. 4a, 4a', 4b, 4b', 4c, 4c', 4d, 4d'). Formation of ternary alloy of GaInP and GaInAs indicates an isosurface map of electron delocalization due to labeling atoms of P/As4, In5, Ga15 (Figs. 4a, 4a'). A vaster jointed area engaged by an isosurface map for Si, Zn, Ag doping GaInP and GaInAs towards formation of heteroclusters of Si@GaInP and Si@GaInAs (Figs. 4b, 4b'), Zn@GaInP and Zn@GaInAs (Figs. 4c, 4c'), Zn@GaInP and Zn@GaInAs (Figs. 4d, 4d') due to labeling atoms of P/As4, Si5/Zn5/Ag5, Ga15, respectively. A narrower connected area occupied by an isosurface map means that electron delocalization is relatively difficult. However, the large counter map of ELF for GaInP, Si@GaInP, Zn@GaInP, Ag@GaInP, GaInAs, Si@GaInAs, Zn@GaInAs, Ag@GaInAs heteroclusters can confirm that doping Ag, Zn, Si nanoparticles on the surface, respectively, increases the efficiency of ternary solar cells of GaInP and GaInAs for energy storage [86–88].

Besides, the changes of charge density analysis have illustrated that GaInP has shown the Bader charge of –0.198 coulomb, and after doping with silicon, zinc and silver has indicated the Bader charge of –0.254, –0.359, –0.167 coulomb for Si@GaInP, Zn@GaInP, Ag@GaInP. Moreover, the changes of charge density analysis have illustrated that GaInAs has shown the Bader charge of –0.240 coulomb, and after doping with silicon, zinc and silver has indicated the Bader charge of –0.201, –0.346, –0.295 coulomb for Si@GaInAs, Zn@GaInAs, Ag@GaInAs, respectively, that describes the more tensity value of these heteroclusters for energy storage [89].

3.2. Theory of Nuclear Quadrupole Resonance (NQR)

The NQR frequencies have been measured for ternary alloys of GaInP, GaInAs and doped heteroclusters of Si@GaInP, Zn@GaInP, Ag@GaInP, Si@GaInAs, Zn@GaInAs, Ag@GaInAs (Table 1). In this research work, the electric potential as the quantity of work energy through carrying over the electric charge from one position to another position in the essence of electric field has been evaluated for GaInP, Si@GaInP, Zn@GaInP, Ag@GaInP, GaInAs, Si@GaInAs, Zn@GaInAs, Ag@GaInAs heteroclusters (Table 1). The atoms of P/As10, P/As14 extracted from ternary heteroclusters of GaInP and GaInAs have exhibited the fluctuation in the range of –1.5 to +1 coulomb with average electric potential about –20 a.u. Then, the hereto clusters of Si@GaInP and Si@GaInAs with active atoms of P/As10, P/As14, P/As16, P/As17 has been oscillated in the range of –1.5 to +1 coulomb with average electric potential about –20 a.u. However, in two hereto-clusters of Zn@GaInP and Zn@GaInAs, the atoms of P/As10, P/As14, P/As14, P/As16, P/As17 have been considered as fluctuated atoms between –1.5 to +1 coulomb with average electric potential about –23 a.u. In fact, by doping transition metals of Zn and Ag to GaInP and GaInAs, the electric potential extracted from NQR calculations grows. Therefore, it can be proposed that doped alloys of Si@GaInP, Zn@GaInP, Ag@GaInP, Si@GaInAs, Zn@GaInAs, Ag@GaInAs might augment the ability of GaInP and GaInAs in solar cells for energy storage.

The two heteroclusters of Zn@GaInP/As and Ag@GaInP/As with the fluctuations of In, Ga, P, As and transition metals of Zn, Ag have indicated the same sensitivity of electric potential. On the other hand, the electrical conductivity based on NQR parameters in Table 1 can be enhanced with doping Zn or Ag. Therefore, it can be considered that zinc and silver atoms in the functionalized Zn@GaInP/As and Ag@GaInP/As might have more impressive sensitivity for accepting the electrons in the process of energy adsorption mechanism.

3.3. Analysis of Nuclear Magnetic Resonance Spectra

Based on the resulted amounts, nuclear magnetic resonance (NMR) spectra of GaInP, Si@GaInP, Zn@GaInP, Ag@GaInP, GaInAs, Si@GaInAs, Zn@GaInAs, Ag@GaInAs heteroclusters as the potential molecules for energy storage can unravel the efficiency of these complexes in solar cells. The NMR data of isotropic (σ_{iso}) and anisotropic shielding tensors (σ_{aniso}) of ternary alloy of GaInP, GaInAs and doped heteroclusters of Si@GaInP, Zn@GaInP, Ag@GaInP, Si@GaInAs, Zn@GaInAs, Ag@GaInAs have been computed by Gaussian 16 revision C.01 program package [40] and been shown in Table 2. NMR data has reported the notable amounts for GaInP, Si@GaInP, Zn@GaInP, Ag@GaInP, GaInAs, Si@GaInAs, Zn@GaInAs, Ag@GaInAs heteroclusters. The notable fragile signal intensity close to the parallel edge of the nanocluster sample might be owing to indium or gallium binding induced non-spherical distribution of GaInP and GaInAs heteroclusters. It exhibited the same tendency of shielding for indium or gallium; however, a considerable deviation exists from doping atoms of silicon, zinc and

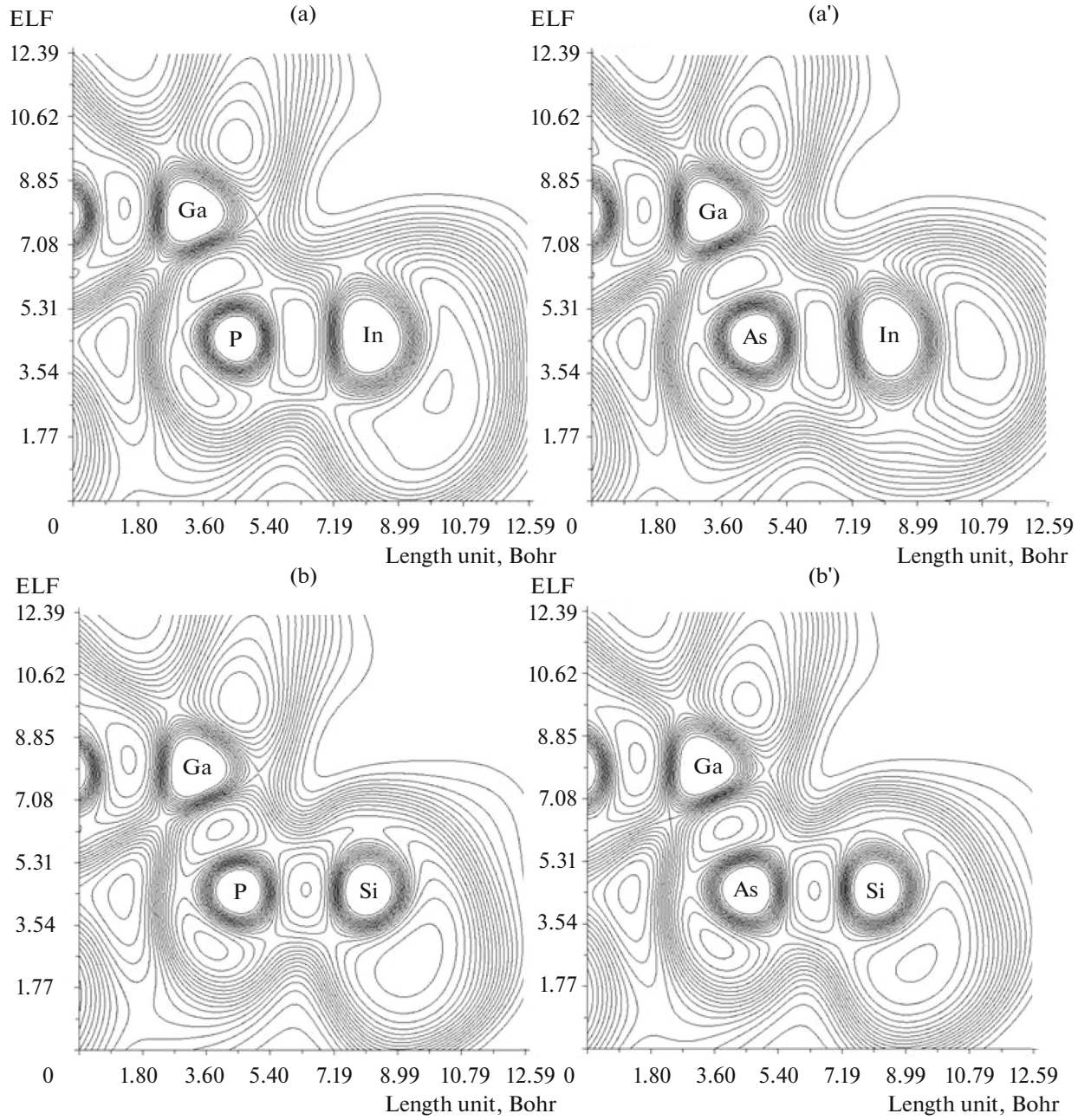

Fig. 4. The graphs of ELF for heteroclusters include (a) GaInP, (a') GaInAs, (b) Si@GaInP, (b') Si@GaInAs, (c) Zn@GaInP, (c') Zn@GaInAs, (d) Ag@GaInP, (d') Ag@GaInAs.

silver as electron acceptors on the surface of GaInP and GaInAs heteroclusters (Table 2).

The yield of electromagnetic shifting can be directed by atoms of P/As10 and P/As14 extracted from ternary hereto clusters of GaInP and GaInAs. Table 2 has shown that the intensity for energy storage can be enhanced in Si@GaInP and Si@GaInAs due to oscillating of chemical shielding in P/As10, P/As14, P/As16, P/As17 atoms. The atoms of P/As10, P/As4, P/As14, P/As16, P/As17 have indicated the fluctuation in chemical shielding for Zn@GaInP/As and Ag@GaInP/As. So, it can be observed that doped heteroclusters of Si@GaInP/As, Zn@GaInP/As and Ag@GaInP/As might ameliorate the capability of $In_4Ga_4N_9$ in solar cells for energy storage.

3.4. Insight of Infrared Spectroscopy and Thermochemistry

The infrared spectroscopy (IR) has been performed for ternary alloy of GaInP, GaInAs and doped heteroclusters of Si@GaInP, Zn@GaInP,

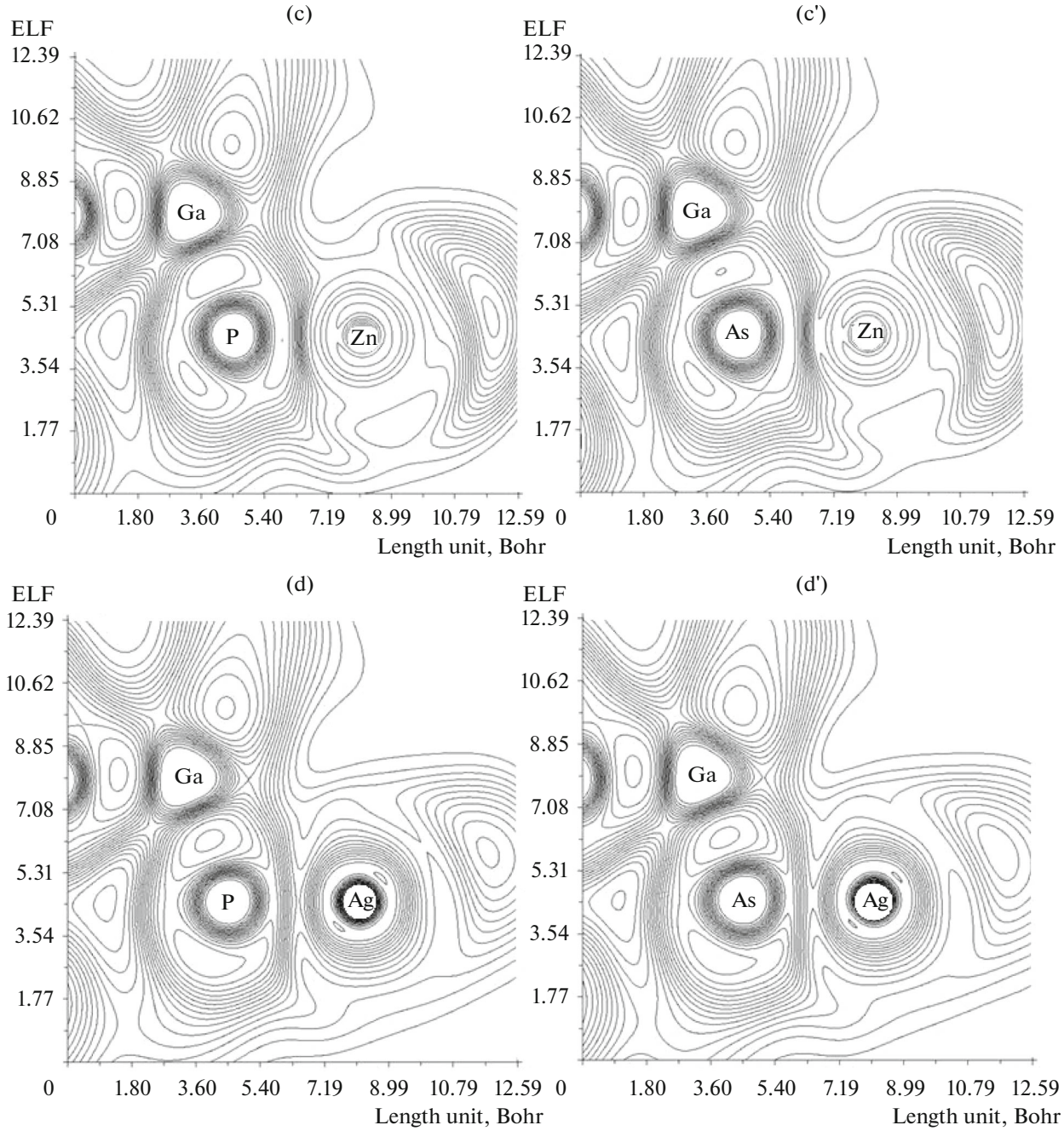

Fig. 4. (Contd.)

Ag@GaInP, Si@GaInAs, Zn@GaInAs, Ag@GaInAs (Figs. 5a, 5a', 5b, 5b', 5c, 5c', 5d, 5d'). Figures 5a–5d has indicated the fluctuation of frequency between 400–2200 cm^{-1} for GaInP, Si@GaInP, Zn@GaInP and Ag@GaInP with sharp peaks around 800 and 2200 cm^{-1}. Furthermore, the fluctuation of frequency between 400–1600 cm^{-1} for GaInAs, Si@GaInAs, Zn@GaInP and Ag@GaInP with sharp peaks around 600 and 1500 cm^{-1} has been found (Figs. 5a'–5d').

Energy storage with heteroclusters has described that the frame of the overcoming cluster is related to Si@GaInP/As, Zn@GaInP/As and Ag@GaInP/As in the high amounts of frequency. This property makes these heteroclusters potentially advantageous for certain high-frequency applications requiring solar cells for energy storage. The advantages of silicon, zinc and silver over gallium indium phosphide and gallium indium arsenide include its higher electron and hole mobility, allowing silver doping devices to operate at

Table 1. The electric potential (E_p/a.u.) and Bader charge (Q/coulomb) through NQR calculation for heteroclusters of GaInP, Si@GaInP, Zn@GaInP, Ag@GaInP, GaInAs, Si@GaInAs, Zn@GaInAs, Ag@GaInAs

GaInP			Si@GaInP			Zn@GaInP			Ag@GaInP		
atom	Q	E_p	atom	Q	E_p	atom	Q	E_p	atom	Q	E_p
Ga1	0.1026	−1.2118	Ga1	0.1047	−1.2039	Ga1	0.1148	−1.2146	Ga1	0.1059	−1.2090
P2	0.1169	−2.7295	P2	−0.1107	−2.7218	P2	−0.1356	−2.7355	P2	−0.1198	−2.7340
In3	0.1511	−1.0479	In3	0.1546	−1.0333	In3	0.1158	−1.0632	In3	0.0663	−1.0634
P4	−0.1682	−2.7542	P4	−0.2542	−2.7455	P4	−0.2580	−2.7767	P4	−0.1137	−2.7460
In5	0.1545	−1.0835	Si5	0.1528	−1.9191	Zn5	0.3590	−16.1738	Ag5	0.0475	−17.8017
Ga6	0.0654	−1.2180	Ga6	0.0674	−1.2054	Ga6	0.0784	−1.2197	Ga6	0.0585	−1.2241
P7	−0.1131	−2.7334	P7	−0.1063	−2.7257	P7	−0.1255	−2.7349	P7	−0.1205	−2.7360
In8	0.1981	−1.0517	In8	0.1988	−1.0448	In8	0.1568	−1.0594	In8	0.1334	−1.0522
P9	−0.0045	−2.7509	P9	−0.0256	−2.7486	P9	−0.0082	−2.7556	P9	−0.0123	−2.7489
P10	−0.0457	−2.8011	P10	−0.0490	−2.7920	P10	−0.0176	−2.7798	P10	−0.0188	−2.7820
Ga11	0.0537	−1.2379	Ga11	0.0734	−1.2309	Ga11	0.0613	−1.2379	Ga11	0.0849	−1.2351
P12	−0.1081	−2.7286	P12	−0.1475	−2.7020	P12	−0.1734	−2.7518	P12	0.0125	−2.7267
In13	−0.1298	−1.1006	In13	−0.0870	−1.0914	In13	−0.1605	−1.0991	In13	−0.1669	−1.0895
P14	−0.0660	−2.7964	P14	−0.0656	−2.7891	P14	−0.0507	−2.7938	P14	−0.0459	−2.7875
Ga15	0.0387	−1.2407	Ga15	0.0659	−1.2331	Ga15	0.0540	−1.2400	Ga15	0.0854	−1.2357
P16	−0.0310	−2.6480	P16	−0.0352	−2.6338	P16	−0.0302	−2.6547	P16	−0.0229	−2.6434
P17	0.0192	−2.6501	P17	0.0636	−2.6311	P17	0.0197	−2.6582	P17	0.0265	−2.6448
GaInAs			Si@GaInAs			Zn@GaInAs			Ag@GaInAs		
atom	Q	E_p	atom	Q	E_p	atom	Q	E_p	atom	Q	E_p
Ga1	0.0418	−1.2092	Ga1	0.0258	−1.1973	Ga1	0.0096	−1.2084	Ga1	0.0241	−1.2016
As2	−0.0748	−2.4958	As2	−0.0553	−2.4882	As2	−0.0664	−2.4990	As2	−0.0559	−2.4995
In3	0.1217	−1.0352	In3	0.1032	−1.0220	In3	0.0818	−1.0426	In3	0.0068	−1.0478
As4	−0.1314	−2.5202	As4	−0.2009	−2.5168	As4	−0.2128	−2.5473	As4	−0.0691	−2.5131
In5	0.1363	−1.0687	Si5	0.1067	−1.9233	Zn5	0.3460	−16.1600	Ag5	0.0406	−17.8014
Ga6	0.0244	−1.2045	Ga6	0.0008	−1.198	Ga6	0.0116	−1.2141	Ga6	−0.0015	−1.2160
As7	−0.0609	−2.4974	As7	−0.0445	−2.4916	As7	−0.0689	−2.5018	As7	−0.0612	−2.5010
In8	0.1452	−1.0427	In8	0.1400	−1.0302	In8	0.1141	−1.0372	In8	0.0703	−1.0363
As9	0.0242	−2.5266	As9	0.0209	−2.5121	As9	0.0661	−2.5138	As9	0.0465	−2.5096
As10	0.0170	−2.5554	As10	0.0039	−2.5551	As10	0.0108	−2.5620	As10	0.0384	−2.5482
Ga11	−0.0086	−1.2263	Ga11	0.0066	−1.2226	Ga11	−0.0173	−1.2331	Ga11	0.0140	−1.2257
As12	−0.0527	−2.4868	As12	−0.0710	−2.4699	As12	−0.1167	−2.5155	As12	0.0668	−2.4984
In13	−0.2405	−1.0817	In13	−0.1729	−1.0715	In13	−0.2810	−1.0799	In13	−0.2954	−1.0708
As14	−0.0078	−2.5582	As14	−0.0191	−2.5561	As14	0.0098	−2.5512	As14	0.0203	−2.5500
Ga15	−0.0170	−1.2257	Ga15	0.0005	−1.2239	Ga15	−0.0098	−1.2307	Ga15	0.0190	−1.2255
As16	0.0041	−2.3759	As16	0.0334	−2.3516	As16	0.0425	−2.3646	As16	0.0377	−2.3629
As17	0.0790	−2.3757	As17	0.1218	−2.3508	As17	0.0805	−2.3693	As17	0.0984	−2.3679

Table 2. Data of NMR shielding tensors (ppm) for selected atoms of heteroclusters containing GaInP, Si@GaInP, Zn@GaInP, Ag@GaInP, GaInAs, Si@GaInAs, Zn@GaInAs, Ag@GaInAs

GaInP			Si@GaInP			Zn@GaInP			Ag@GaInP		
atom	σ_{iso}	σ_{aniso}	atom	σ_{iso}	σ_{aniso}	atom	σ_{iso}	σ_{aniso}	atom	σ_{iso}	σ_{aniso}
Ga1	2.9912	16.4084	Ga1	14.7085	140.2988	Ga1	5.7833	14.5749	Ga1	3.7750	34.4763
P2	16.2010	40.6634	P2	68.4834	625.8891	P2	30.2094	47.7035	P2	22.9294	18.0919
In3	3.1564	15.8887	In3	131.7170	427.4682	In3	7.9646	11.9775	In3	3.6760	11.4878
P4	22.7075	60.8319	P4	804.6769	1389.8580	P4	36.5989	41.5291	P4	47.5503	27.4761
In5	10.9969	13.8506	Si5	2860.3818	5164.8465	Zn5	9.3438	226.6506	Ag5	393.5721	558.6332
Ga6	1.2904	24.4243	Ga6	267.4956	566.4396	Ga6	9.2207	17.2757	Ga6	2.9683	6.6546
P7	17.2864	58.4028	P7	16.2609	542.0997	P7	25.2067	38.3781	P7	24.0390	19.4948
In8	4.9301	14.9211	In8	9.0080	97.6623	In8	4.7382	12.3749	In8	8.3272	23.2560
P9	28.8631	25.4405	P9	91.8204	246.9075	P9	37.5249	47.2443	P9	58.9997	117.4414
P10	30.7698	116.3719	P10	503.5063	1881.0068	P10	8.5079	171.6037	P10	60.6719	105.9426
Ga11	6.3168	13.0068	Ga11	50.1587	319.1833	Ga11	7.0744	9.5749	Ga11	0.2429	18.3864
P12	9.1231	22.0187	P12	884.9371	1426.2068	P12	14.2417	29.1589	P12	75.2296	156.3703
In13	5.6051	14.0973	In13	58.6594	165.8298	In13	7.9784	16.4409	In13	8.8481	26.4861
P14	58.3719	117.9195	P14	322.0308	1477.9439	P14	51.7048	178.1570	P14	60.3844	116.8811
Ga15	6.1193	14.0998	Ga15	115.3250	362.1296	Ga15	5.7509	10.6229	Ga15	1.2247	19.7986
P16	17.2493	20.2584	P16	75.5403	269.6551	P16	13.3250	15.1974	P16	52.6745	55.9966
P17	16.5831	31.6549	P17	111.5741	550.4411	P17	9.9093	27.4979	P17	13.2274	25.9349
GaInAs			Si@GaInAs			Zn@GaInAs			Ag@GaInAs		
atom	σ_{iso}	σ_{aniso}	atom	σ_{iso}	σ_{aniso}	atom	σ_{iso}	σ_{aniso}	atom	σ_{iso}	σ_{aniso}
Ga1	0.3074	22.0861	Ga1	0.0792	15.9341	Ga1	0.6750	21.1703	Ga1	0.7520	19.8593
As2	29.8236	19.6313	As2	25.3146	28.6917	As2	23.1833	28.7591	As2	29.3266	14.1258
In3	6.9570	15.2904	In3	4.0747	36.0498	In3	9.8905	16.7811	In3	5.4711	11.9363
As4	31.1679	42.1877	As4	26.3934	58.6309	As4	37.8469	30.5219	As4	34.4168	33.3078
In5	6.5331	26.0498	Si5	82.2563	134.8817	Zn5	28.1128	258.0039	Ag5	264.0270	198.3803
Ga6	4.9931	21.3464	Ga6	1.0019	48.1536	Ga6	11.0560	27.7590	Ga6	3.9803	10.8326
As7	29.2555	20.4417	As7	25.7353	29.6306	As7	37.7734	43.6597	As7	29.3101	14.7364
In8	3.2540	15.6435	In8	3.7465	12.1451	In8	10.0028	17.3503	In8	4.9978	14.0723
As9	33.1441	18.2773	As9	33.2210	29.1774	As9	37.1966	37.6456	As9	34.0167	16.5118
As10	1.5355	38.3636	As10	4.2091	50.1160	As10	87.3312	281.8346	As10	7.5991	55.2786
Ga11	8.5234	16.2496	Ga11	9.7332	22.7859	Ga11	12.4382	26.1392	Ga11	4.9066	9.7615
As12	20.4792	16.4775	As12	4.8271	41.5559	As12	16.7441	28.0545	As12	9.4031	63.4163
In13	13.9073	6.6538	In13	3.6415	12.8873	In13	10.8811	28.1587	In13	3.2084	14.9917
As14	5.2686	38.8713	As14	0.8467	70.3439	As14	16.6354	217.0360	As14	7.1376	59.5777
Ga15	8.8580	15.0711	Ga15	9.4986	22.0994	Ga15	4.8167	21.5119	Ga15	4.0903	10.4577
As16	19.6123	28.1556	As16	16.1567	18.0408	As16	17.2297	24.7023	As16	34.4048	21.6306
As17	16.0551	27.6943	As17	19.0565	9.8546	As17	1.8169	24.5890	As17	18.6066	19.6882

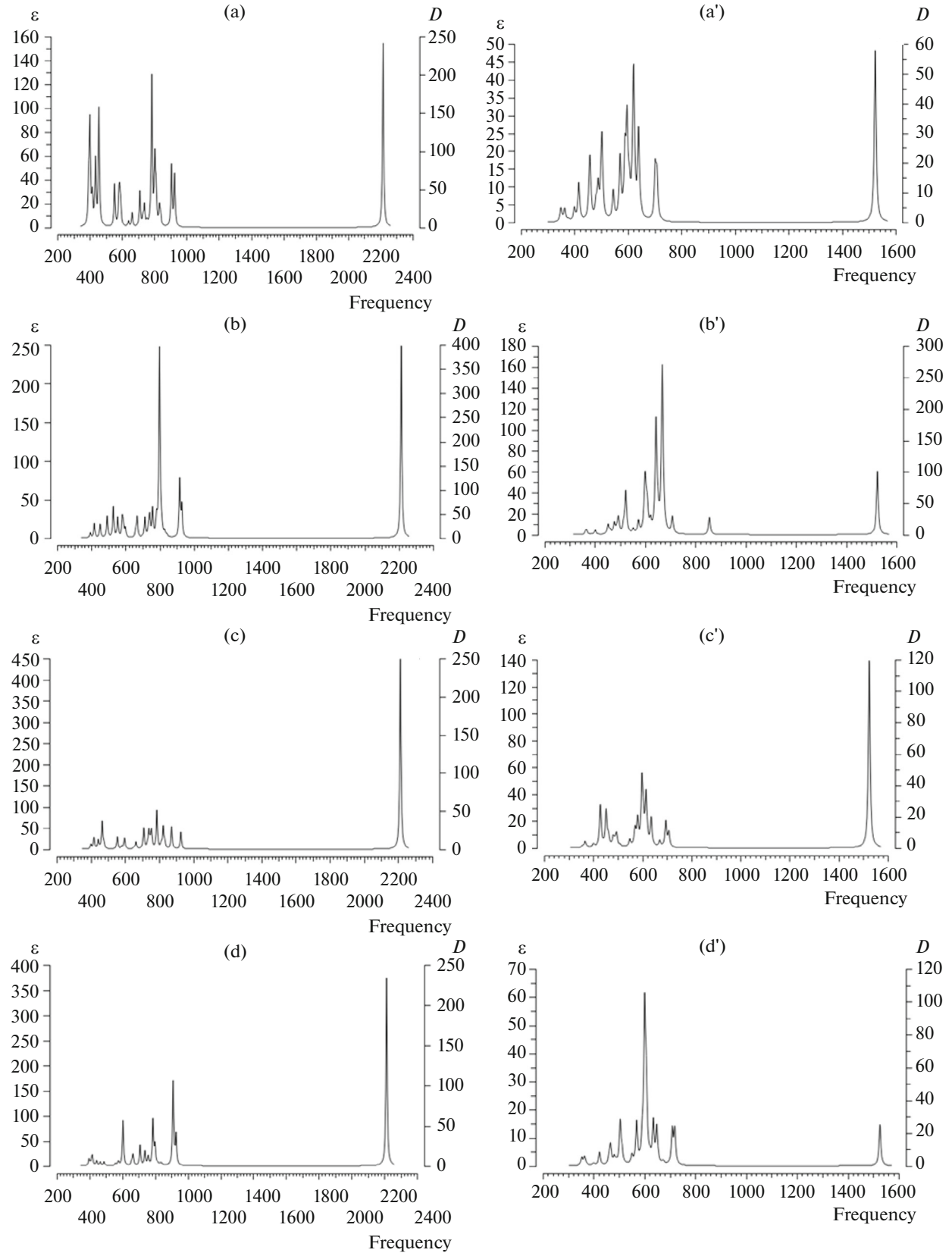

Fig. 5. The frequency (cm^{-1}) changes through the IR spectra for heteroclusters of (a) GaInP, (a') GaInAs, (b) Si@GaInP, (b') Si@GaInAs, (c) Zn@GaInP, (c') Zn@GaInAs, (d) Ag@GaInP, (d') Ag@GaInAs. Note: ε ($M^{-1}cm^{-1}$ or $Lmol^{-1}cm^{-1}$) is the absorbance unit and D (10^{-4} esu^2 cm^2) is the dipole strength via the esu or electrostatic unit, which is a unit of charge in the cgs (centimeter-gram-second) system.

Table 3. The thermodynamic characters of heteroclusters of GaInP, Si@GaInP, Zn@GaInP, Ag@GaInP, GaInAs, Si@GaInAs, Zn@GaInAs, Ag@GaInAs using CAM–B3LYP–D3/6-311+G(*d*, *p*) calculation

Compound	Dipole moment, D	$\Delta E_f^o \times 10^{-3}$, kcal/mol	$\Delta H_f^o \times 10^{-3}$, kcal/mol	$\Delta G_f^o \times 10^{-3}$, kcal/mol	S_{ads}^o, cal/K mol	$E_{atom\text{-}doping}^o$, kcal/mol
GaInP	8.2065	−44.7046	−44.7041	−44.7324	94.915	–
Si@GaInP	9.2277	−46.0130	−46.0124	−46.0399	92.431	−1.3084
Zn@GaInP	7.1636	−84.6627	−84.6621	−84.6898	93.069	−39.9581
Ag@GaInP	7.0827	−134.9798	−134.9792	−135.0074	94.694	−90.2752
GaInAs	6.8245	−41.9156	−41.9150	−41.9452	101.109	–
Si@GaInAs	8.4976	−43.2327	−43.2321	−43.2615	98.570	−1.3171
Zn@GaInAs	7.1003	−81.8811	−81.8805	−81.9102	99.358	−39.9655
Ag@GaInAs	6.3828	−132.1937	−132.1931	−132.2232	100.844	−90.2781

higher frequencies than silicon and zinc doping devices [90].

Table 3 through the thermodynamic specifications concluded that heteroclusters of GaInP, Si@GaInP, Zn@GaInP, Ag@GaInP, GaInAs, Si@GaInAs, Zn@GaInAs, Ag@GaInAs might be more efficient structure for energy storage in the solar cells. Thermodynamic parameters of heteroclusters of Si@GaInP, Zn@GaInP, Ag@GaInP, Si@GaInAs, Zn@GaInAs, Ag@GaInAs have been assigned through doping of ternary alloys of GaInP and GaInAs with Si, Zn and Ag towards formation heteroclusters (Table 3).

The adsorption efficiency of GaInP, Si@GaInP, Zn@GaInP, Ag@GaInP, GaInAs, Si@GaInAs, Zn@GaInAs, Ag@GaInAs based on dipole moment has been evaluated by the ΔG_f^o. The changes of Gibbs free energy versus dipole moment could detect the maximum efficiency of Ag@GaInP and Ag@GaInAs heteroclusters for energy storage in the solar cells through $\Delta G_{f,Ag@GaInP}^o = -134.9792 \times 10^3$ kcal/mol and $\Delta G_{f,Ag@GaInAs}^o = -132.1931 \times 10^3$ kcal/mol, respectively (Table 3). Moreover, In GaInP and GaInAs, the photo excited electrons and holes are strongly bounded by the excitons because of their large exciton binding energy as $E_{Ag@GaInX}^o > E_{Zn@GaInX}^o > E_{Si@GaInX}^o$ (X = P or As) due to its efficient exciton dissociation (Table 3).

The solar cells formed by GaInP, Si@GaInP, Zn@GaInP, Ag@GaInP, GaInAs, Si@GaInAs, Zn@GaInAs, Ag@GaInAs feature a hierarchical structure with the electron donor/acceptor layer sandwiched by anode and cathode, which raises the importance of controlling the molecular crystal orientation, domain size, and vertical distribution to facilitate the charge collection at electrodes. Doping obviously reduces indium atoms composition, the aggregation of In–In and induces the deep energy level. This greatly decreases the defects and improves the valence band potential of GaInP and GaInAs nanorods. In this paper, it was demonstrated that the ternary semiconductors of gallium indium phosphide and gallium indium arsenide can lead to a significant absorption enhancement in a broad spectral range of incident light in the presence of silicon, zinc or silver. A comparison between solar cells containing Si-, Zn- or Ag-doped GaInP or GaInAs shows that the solar cells containing Zn or Ag structures show a more enhanced solar cell performance than the solar cells containing only the single GaInP or GaInAs structure. This efficient doping strategy not only bridges the gaps of heteroatom doped GaInP or GaInAs based photoelectrodes but also can provide deep insights into controlling the electronic structure for enhanced solar converting efficiency [91].

4. CONCLUSIONS

In this investigation, it has been provided a ternary semiconductors of gallium indium phosphide and gallium indium arsenide which are doped with silicon, zinc or silver. Energy grabbing on the heteroclusters of Si@GaInP, Zn@GaInP, Ag@GaInP, Si@GaInAs, Zn@GaInAs, Ag@GaInAs in solar cells was investigated by first-principles calculations. The effect of a relative chemical shift between GaInP, GaInAs and doped heteroclusters of the solar cell was also investigated. Thermodynamic parameters have constructed a detailed molecular model for atom–atom interactions and a distribution of point charges which can be utilized to reproduce the polarity of the solid material and the adsorbing molecules. In GaInP and GaInAs, the photo excited electrons and holes are strongly bounded by the excitons because of their large exciton binding energy as $E_{Ag@GaInX}^o > E_{Zn@GaInX}^o > E_{Si@GaInX}^o$ (X = P or As) due to its efficient exciton dissociation.

The two heteroclusters of Zn@GaInP/As and Ag@GaInP/As with the fluctuations of In, Ga, P, As and transition metals of Zn, Ag have indicated the same sensitivity of electric potential. On the other hand, the electrical conductivity based on NQR

parameters can be enhanced by doping Zn or Ag. The advantages of silver over gallium indium phosphide and gallium indium arsenide include its higher electron and hole mobility, allowing silver doping devices to operate at higher frequencies than silicon and zinc doping devices through $\Delta G^{o}_{f,Ag@GaInP} = -134.9792 \times 10^3$ kcal/mol and $\Delta G^{o}_{f,Ag@GaInAs} = -132.1931 \times 10^3$ kcal/mol, respectively. Thus, it should be explored its unique properties, such as its ability to increase energy storage which could lead to advancements in solar cells. III–V multijunction semiconductor solar cells have leading photoelectric conversion efficiency relative to other materials, suitable for applications with high-efficiency requirements. This article can characterize the functional lattice matched of (Si, Zn, Ag)-Doped GaInP/GaInAs solar cells as a proposed efficient storage of energy.

ACKNOWLEDGMENTS

In successfully completing this paper and its research, the author is grateful to Kastamonu University.

FUNDING

This work was supported by ongoing institutional funding. No additional grants to carry out or direct this particular research were obtained.

CONFLICT OF INTEREST

The author of this work declares that he has no conflicts of interest.

REFERENCES

1. A. Di Carlo, Phys. Status Solidi A **183**, 81–85 (2001). https://doi.org/10.1002/1521-396X(200101)183:1<81::AID-PSSA81>3.0.CO;2-N
2. Y. Arakawa, IEEE J. Select. Top. Quantum Electron. **8**, 823–832 (2002). https://doi.org/10.1109/JSTQE.2002.801675
3. L. V. Lukin, Russ. J. Phys. Chem. B **17**, 1300–1308 (2023). https://doi.org/10.1134/S1990793123060180
4. M. G. Golubkov, A. V. Dmitriev, A. V. Suvorova, et al., Russ. J. Phys. Chem. B **16**, 537–542 (2022). https://doi.org/10.1134/S199079312203006X
5. Q. Meng, Q. Lin, F. Han, et al., Materials **14**, 6193 (2021). https://doi.org/10.3390/ma14206193
6. F. Mollaamin and M. Monajjemi, Russ. J. Phys. Chem. B **18**, 1199–1216 (2024). https://doi.org/10.1134/S1990793124700519
7. M. Monajjemi, F. Mollaamin, S. Shahriari, et al., Russ. J. Phys. Chem. B **18**, 1090–1112 (2024). https://doi.org/10.1134/S1990793124700465
8. F. Mollaamin and M. Monajjemi, Russ. J. Phys. Chem. B **18**, 1177–1198 (2024). https://doi.org/10.1134/S1990793124700507
9. H. Amano, N. Sawaki, I. Akasaki, et al., Appl. Phys. Lett. **48**, 353 (1986). https://doi.org/10.1063/1.96549
10. F. Mollaamin and M. Monajjemi, Russ. J. Phys. Chem. B **18**, 533–548 (2024). https://doi.org/10.1134/S199079312402012X
11. H. Amano, M. Kito, K. Hiramatsu, et al., Jpn. J. Appl. Phys. **28**, L2112 (1989). https://doi.org/10.1143/JJAP.28.L2112
12. H. Amano, T. Asahi, and I. Akasaki, Jpn. J. Appl. Phys. **29**, L205 (1990). . https://doi.org/10.1143/JJAP.29.L205
13. I. Akasaki, H. Amano, S. Sota, et al., Jpn. J. Appl. Phys. **34**, L1517 (1995). https://doi.org/10.7567/JJAP.34.L1517
14. M. Kodama, M. Sugimoto, E. Hayashi, et al., Appl. Phys. Express **1**, 021104 (2008). https://doi.org/10.1143/APEX.1.021104
15. M. Wraback, H. Shen, J. C. Carrano, et al., Appl. Phys. Lett. **76**, 1155–1157 (2000). https://doi.org/10.1063/1.125968
16. L. I. Trakhtenberg, M. I. Ikim, O. J. Ilegbusi, et al., Chemosensors **11**, 320 (2023). https://doi.org/10.3390/chemosensors11060320
17. R. J. Bashirov, N. E. Ismayilov, R. E. Huseynov, et al., Adv. Phys. Res. **6**, 90–99 (2024). https://doi.org/10.62476/apr62.90
18. Sh. B. Utamuradova, Sh. Kh. Daliev, B. R. Bokiev, et al., Adv. Phys. Res. **6**, 211–218 (2024). https://doi.org/10.62476/apr63211
19. Sh. B. Utamuradova, D. A. Rakhmanov, P. L. Tuan, et al., Adv. Phys. Res. **6**, 83–89 (2024). https://doi.org/10.62476/apr62.83
20. L. K. Abdullayeva and M. H. Hasanov, New Mater., Compd. Appl. **8**, 135–141 (2024). https://doi.org/10.62476/nmca8135
21. A. F. Noori, A. M. Ghaleb, and A. I. Salih, Adv. Phys. Res. **6**, 225–238 (2024). https://doi.org/10.62476/apr63225
22. A. F. Gochuyeva, A. M. Mehdiyeva, and S. V. Bakhshaliyeva, New Mater., Compd. Appl. **8**, 87–93 (2024). https://doi.org/10.62476/nmca8187
23. C. J. Neufeld, S. C. Cruz, R. M. Farrell, et al., Appl. Phys. Lett. **98**, 243507 (2011). https://doi.org/10.1063/1.3595487
24. K. V. Zolotarev, A. N. Mikhailov, V. I. Nakhod, et al., New Mater., Compd. Appl. **8**, 162–170 (2024). https://doi.org/10.62476/nmca82162
25. K. X. Wang, Z. Yu, V. Liu, et al., Nano Lett. **12**, 1616–1619 (2012). https://doi.org/10.1021/nl204550q
26. X. Meng, E. Drouard, G. Gomard, et al., Opt Express. **20**, A560–A571 (2012). https://doi.org/10.1364/OE.20.00A560
27. A. Abass, K. Q. Le, A. Alu, et al., Phys. Rev. B **85**, 115449 (2012). https://doi.org/10.1103/PhysRevB.85.115449

28. R. Chriki, A. Yanai, J. Shappir, et al., Opt. Express **21**, A382–A391 (2013). https://doi.org/10.1364/OE.21.00A382
29. W. C. Hsu, J. K. Tong, M. S. Branham, et al., Opt. Commun. **377**, 52–58 (2016). https://doi.org/10.1016/j.optcom.2016.04.055
30. O. Isabella, R. Vismara, A. Ingenito, et al., Opt. Express. **24**, A708–A719 (2016). https://doi.org/10.1364/OE.24.00A708
31. K. Kourchid, R. Alaya, N. Bouguila, et al., Russ. J. Phys. Chem. B **18**, 37–48 (2024). https://doi.org/10.1134/S1990793124010317
32. M. Monajjemi, F. Mollaamin, S. Shahriari, et al., Russ. J. Phys. Chem. B **18**, 1217–1225 (2024). https://doi.org/10.1134/S1990793124700349
33. I. Asfour, Russ. J. Phys. Chem. B **18**, 83–94 (2024). https://doi.org/10.1134/S1990793124010032
34. Y.-C. Pu, M. G. Kibria, Z. Mi, et al., J. Phys. Chem. Lett. **6**, 2649–2656 (2015). https://doi.org/10.1021/acs.jpclett.5b00909
35. M. L. Reed, E. A. Berkman, M. J. Reed, et al., MRS Online Proceedings Library **798**, 742–747 (2003). https://doi.org/10.1557/PROC-798-Y8.6
36. W. Zhang, R. Deng, M. Luo, et al., AIP Adv. **14**, 045301 (2024). https://doi.org/10.1063/5.0202164
37. J. Lin, Y. Yu, Z. Xu, et al., J. Power Sources **450**, 227578 (2020). https://doi.org/10.1016/j.jpowsour.2019.227578
38. M. I. Ikim, E. Yu. Spiridonova, V. F. Gromov, et al., Russ. J. Phys. Chem. B **18**, 283–288 (2024). https://doi.org/10.1134/S199079312401010X
39. M. I. Ikim, E. Yu. Spiridonova, V. F. Gromov, et al., Russ. J. Phys. Chem. B **17**, 774–777 (2023). https://doi.org/10.1134/S199079312303003X
40. G. N. Gerasimov, V. F. Gromov, O. J. Ilegbusi, et al., Sens. Actuators B **240**, 613–624 (2017). https://doi.org/10.1016/j.snb.2016.09.007
41. U. K. Kumawat, K. Kumar, P. Bhardwaj, et al., Energy Sci. Eng. **7**, 2469–2482 (2019). https://doi.org/10.1002/ese3.436
42. F. Mollaamin and M. Monajjemi, Russ. J. Phys. Chem. B **18**, 49–66 (2024). https://doi.org/10.1134/S1990793124010159
43. B. Khalili Hadad, F. Mollaamin, and M. Monajjemi, Russ. Chem. Bull. **60**, 238–241 (2011). https://doi.org/10.1007/s11172-011-0039-5
44. F. Mollaamin and M. Monajjemi, J. Cluster Sci. **34**, 2901–2918 (2023). https://doi.org/10.1007/s10876-023-02436-5
45. M. Monajjemi, F. Mollaamin, and S. Shojaei, Biointerface Res. Appl. Chem. **10**, 5575 (2020). https://doi.org/10.33263/BRIAC103.575585
46. F. Mollaamin, S. Shahriari, M. Monajjemi, et al., J. Cluster Sci. **34**, 1547–1562 (2023). https://doi.org/10.1007/s10876-022-02335-1
47. M. Monajjemi, S. Mohammadi, S. Shahriari, et al., Russ. J. Phys. Chem. B **18**, 308–324 (2024). https://doi.org/10.1134/S1990793124010342
48. F. Mollaamin and M. Monajjemi, J. Mol. Model. **29**, 170 (2023). https://doi.org/10.1007/s00894-023-05567-8
49. F. Mollaamin, S. Mohammadi, Z. Khalaj, et al., Russ. J. Phys. Chem. B **18**, 67–82 (2024). https://doi.org/10.1134/S1990793124010330
50. M. Monajjemi and F. Mollaamin, Energies **17**, 4530 (2024). https://doi.org/10.3390/en17184530
51. F. Mollaamin and M. Monajjemi, Sensor Rev. **43**, 266–279 (2023). https://doi.org/10.1108/SR-03-2023-0040
52. F. Mollaamin and M. Monajjemi, C—J. Carbon Res. **9**, 20 (2023). https://doi.org/10.3390/c9010020
53. M. Monajjemi, M. Khaleghian, N. Tadayonpour, et al., Int. J. Nanosci. **9**, 517–529 (2010). https://doi.org/10.1142/S0219581X10007071
54. F. Mollaamin and M. Monajjemi, Int. J. Quantum Chem. **124**, e27348 (2024). https://doi.org/10.1002/qua.27348
55. F. Mollaamin and M. Monajjemi, Mol. Simul. **49**, 365–376 (2023). https://doi.org/10.1080/08927022.2022.2159996
56. M. J. Frisch, G. W. Trucks, H. B. Schlegel, G. E. Scuseria, M. A. Robb, J. R. Cheeseman, G. Scalmani, V. Barone, G. A. Petersson, H. Nakatsuji, X. Li, M. Caricato, A. V. Marenich, J. Bloino, B. G. Janesko, R. Gomperts, B. Mennucci, H. P. Hratchian, J. V. Ortiz, A. F. Izmaylov, J. L. Sonnenberg, D. Williams-Young, F. Ding, F. Lipparini, F. Egidi, J. Goings, B. Peng, A. Petrone, T. Henderson, D. Ranasinghe, V. G. Zakrzewski, J. Gao, N. Rega, G. Zheng, W. Liang, M. Hada, M. Ehara, K. Toyota, R. Fukuda, J. Hasegawa, M. Ishida, T. Nakajima, Y. Honda, O. Kitao, H. Nakai, T. Vreven, K. Throssell, J. A. Montgomery, Jr., J. E. Peralta, F. Ogliaro, M. J. Bearpark, J. J. Heyd, E. N. Brothers, K. N. Kudin, V. N. Staroverov, T. A. Keith, R. Kobayashi, J. Normand, K. Raghavachari, A. P. Rendell, J. C. Burant, S. S. Iyengar, J. Tomasi, M. Cossi, J. M. Millam, M. Klene, C. Adamo, R. Cammi, J. W. Ochterski, R. L. Martin, K. Morokuma, O. Farkas, J. B. Foresman, and D. J. Fox, Gaussian 16, Revision C.01 (Gaussian, Inc., Wallingford, CT, 2016).
57. R. Dennington, T. A. Keith, and J. M. Millam, GaussView, Version 6.06.16 (Semichem Inc., Shawnee Mission, KS, 2016).
58. F. Mollaamin and M. Monajjemi, Comput. Theor. Chem. **1237**, 114646 (2024). https://doi.org/10.1016/j.comptc.2024.114646
59. R. Sciotto, I. A. Ruiz Alvarado, and W. G. Schmidt, Surfaces **7**, 79–87 (2024). . https://doi.org/10.3390/surfaces7010006
60. J. Luo, C. Wang, Z. Wang, et al., Chin. Phys. B **29**, 067402 (2020). https://doi.org/10.1088/1674-1056/ab892d
61. F. Mollaamin and M. Monajjemi, J. Mol. Struct. **1300**, 137214 (2024). https://doi.org/10.1016/j.molstruc.2023.137214

62. F. Mollaamin and M. Monajjemi, Phys. Chem. Liq. **50**, 596–604 (2012). https://doi.org/10.1080/00319104.2011.646444
63. M. A. A. Zadeh, H. Lari, L. Kharghanian, et al., J. Comput. Theor. Nanosci. **12**, 4358 (2015). https://doi.org/10.1166/jctn.2015.4366
64. M. Monajjemi, S. Afsharnezhad, M. R. Jaafari, et al., Chemistry **17**, 55–69 (2008).
65. K. Bakhshi, F. Mollaamin and M. Monajjemi, J. Comput. Theor. Nanosci. **8**, 763–768 (2011). https://doi.org/10.1166/jctn.2011.1750
66. M. Monajjemi, A. Sobhanmanesh, and F. Mollaamin, Fullerenes Nanotubes Carbon Nanostruct. **21**, 47–63 (2013). https://doi.org/10.1080/1536383X.2011.574325
67. F. Mollaamin and M. Monajjemi, J. Mol. Model. **29**, 119 (2023). https://doi.org/10.1007/s00894-023-05526-3
68. F. Mollaamin and M. Monajjemi, Comput. Theor. Chem. **1237**, 114666 (2024). https://doi.org/10.1016/j.comptc.2024.114666
69. V. Ya. Agroskin, B. G. Bravy, G. K. Vasiliev, et al., Russ. J. Phys. Chem. B **17**, 1265–1269 (2023). https://doi.org/10.1134/S1990793123060131
70. L. I. Trakhtenberg, Russ. J. Phys. Chem. B **17**, 600–607 (2023). https://doi.org/10.1134/S1990793123030144
71. V. A. Aleksandrova and A. M. Futoryanskaya, Russ. J. Phys. Chem. B **17**, 1394–1397 (2023). https://doi.org/10.1134/S1990793123060143
72. Z. Xu, C. Qin, Y. Yu, et al., AIP Adv. **14**, 055114 (2024). https://doi.org/10.1063/5.0208082
73. N. M. O'Boyle, A. L. Tenderholt, and K. M. Langner. J. Comput. Chem. **29**, 839–845 (2008). https://doi.org/10.1002/jcc.20823
74. T. Lu and F. Chen, J. Comput. Chem. **33**, 580–592 (2012). https://doi.org/10.1002/jcc.22885
75. T. Lu, J. Chem. Phys. **161**, 082503 (2024). https://doi.org/10.1063/5.0216272
76. A. D. Becke and K. E. Edgecombe, J. Chem. Phys. **9**, 5397–5403 (1990). https://doi.org/10.1063/1.458517
77. S. N. Steinmann, Y. Mob, and C. Corminboeuf, Phys. Chem. Chem. Phys. **13**, 20584–20592 (2011). https://doi.org/10.1039/C1CP21055F
78. L. Tian, C. Feiwu, and W. Xuebao, Acta Phys. Chim. Sin. **27**, 2786–2792 (2011). https://doi.org/10.3866/PKU.WHXB20112786
79. F. Mollaamin and M. Monajjemi, Russ. J. Phys. Chem. B **17**, 658–672 (2023). https://doi.org/10.1134/S1990793123030223
80. A. Savin, O. Jepsen, J. Flad, et al., Angew. Chem. Int. Ed. Engl. **31**, 187 (1992). https://doi.org/10.1002/anie.199201871
81. F. Mollaamin, J. Comput. Theor. Nanosci. **11**, 2393–2398 (2014). https://doi.org/10.1166/jctn.2014.3653
82. M. Monajjemi, H. Yamola and F. Mollaamin, Fullerenes Nanotubes Carbon Nanostruct. **22**, 595–603 (2014). https://doi.org/10.1080/1536383X.2012.702163
83. F. Mollaamin, F. Najafi, M. Khaleghian, B. Khalili Hadad, and M. Monajjemi, Fullerenes Nanotubes Carbon Nanostruct. **19**, 653–667 (2011). https://doi.org/10.1080/1536383X.2010.504956
84. S. Shahriari, F. Mollaamin, and M. Monajjemi, Micromachines **14**, 241 (2023). https://doi.org/10.3390/mi14020241
85. F. Mollaamin and M. Monajjemi, J. Bio- Tribo-Corros. **9**, 33 (2023). https://doi.org/10.1007/s40735-023-00751-y
86. F. Mollaamin, Russ. J. Phys. Chem. B **18**, 805–820 (2024). https://doi.org/10.1134/S1990793124700131
87. V. V. Parakhin, V. M. Volokhov, E. S. Amosova, et al., Russ. J. Phys. Chem. B **18**, 697–706 (2024). https://doi.org/10.1134/S1990793124700088
88. F. Mollaamin, S. Shahriari, and M., Russ. J. Phys. Chem. B **18**, 398–418 (2024). https://doi.org/10.1134/S199079312402026X
89. F. Mollaamin and M. Monajjemi, Russ. J. Phys. Chem. B **18**, 607–623 (2024). https://doi.org/10.1134/S1990793124020271
90. F. Mollaamin, M. Monajjemi, J. Comput. Theor. Nanosci. **9**, 597–601 (2012). https://doi.org/10.1166/jctn.2012.2067
91. E. F. Nemova, T. V. Kobzeva, and G. G. Dultseva, Russ. J. Phys. Chem. B **18**, 95–100 (2024). https://doi.org/10.1134/S1990793124010354